AFRL-AFOSR-JP-TR-2019-0005

Photonic MMW monopulse radar with ultra-wide bandwidth chirped pulse for high-resolution 3-D imagine

Jin Wei Shi
NATIONAL CENTRAL UNIVERSITY
300, JHONGDA RD.
CHUNGLI CITY, 32001
TW

02/09/2019
Final Report

Air Force Research Laboratory
Air Force Office of Scientific Research
Asian Office of Aerospace Research and Development
Unit 45002, APO AP 96338-5002

REPORT DOCUMENTATION PAGE

Form Approved
OMB No. 0704-0188

1. REPORT DATE *(DD-MM-YYYY)*	2. REPORT TYPE	3. DATES COVERED *(From - To)*
09-02-2019	Final	09 Dec 2016 to 08 Dec 2017

4. TITLE AND SUBTITLE
Photonic MMW monopulse radar with ultra-wide bandwidth chirped pulse for high-resolution 3-D imagine

5a. CONTRACT NUMBER

5b. GRANT NUMBER
FA2386-17-1-0033

5c. PROGRAM ELEMENT NUMBER
61102F

6. AUTHOR(S)
Jin Wei Shi

5d. PROJECT NUMBER

5e. TASK NUMBER

5f. WORK UNIT NUMBER

7. PERFORMING ORGANIZATION NAME(S) AND ADDRESS(ES)
NATIONAL CENTRAL UNIVERSITY
300, JHONGDA RD.
CHUNGLI CITY, 32001 TW

8. PERFORMING ORGANIZATION REPORT NUMBER

9. SPONSORING/MONITORING AGENCY NAME(S) AND ADDRESS(ES)
AOARD
UNIT 45002
APO AP 96338-5002

10. SPONSOR/MONITOR'S ACRONYM(S)
AFRL/AFOSR IOA

11. SPONSOR/MONITOR'S REPORT NUMBER(S)
AFRL-AFOSR-JP-TR-2019-0005

12. DISTRIBUTION/AVAILABILITY STATEMENT
A DISTRIBUTION UNLIMITED: PB Public Release

13. SUPPLEMENTARY NOTES

14. ABSTRACT
This project improved the output MMW power, MMW bandwidth, and reliability of photonic emitter itself. Also, demonstrate sum and difference antenna-patterns with a large operation bandwidth (75-110 GHz; full W-band) by use of advanced optical signal processing technique onto newly developed emitter array.

15. SUBJECT TERMS
near-ballistic uni-traveling-carrier, photodiode, photonic emitter, photo-generated MMW, monopulse radar.

16. SECURITY CLASSIFICATION OF:			17. LIMITATION OF ABSTRACT	18. NUMBER OF PAGES	19a. NAME OF RESPONSIBLE PERSON
a. REPORT	b. ABSTRACT	c. THIS PAGE			KIM, TONY
Unclassified	Unclassified	Unclassified	SAR		19b. TELEPHONE NUMBER *(Include area code)* 315-227-7008

Photonic MMW monopulse radar with ultra-wide bandwidth chirped pulse for high-resolution 3-D imagine

(From 2016/12/08 to 2017/12/07)

FA2386-17-1-0033/AFRL-AFOSR-JP-TR-2019 0005

Investigators:

Joint People:

1. Prof. Jin-Wei Shi at National Central University, Taiwan
2. Prof. Andy Weiner at Purdue University, IN, USA
3. Dr. Daniel E. Leaird at Purdue University, IN, USA
4. Prof. Nan-Wei Chen at Yuan Ze University, Taiwan

Email: jwshi@ee.ncu.edu.tw (project instructor)

Abstract:

By combing novel ultra-wide bandwidth (>100 GHz) and high-power photonic emitter at sub-THz regime with advanced optical pulse shaper technology, we will demonstrate a photonic monopulse radar with ultra-wide bandwidth of chirped pulse for high-resolution 3-D imagine.

Introduction:

The real time millimeter-wave (MMW) arbitrary waveform generation remains a challenge in now day due to the limited bandwidth of electrical arbitrary waveform generator (AWG). By use of the photonic approach, such as optical pulse shaper is a powerful solution to achieve such goal. Several optical shaper based AWG at microwave band has been demonstrated. However, the frequency resolution and dynamic response (frequency sweeping time) of this approach are still hard to be competed with the existed electrical solution in microwave frequency regime. On the other hand, in order to convert the optical MMW envelope into high-power MMW signal for practical application, a high-power photodiode (PD) with ultra-wide (> 100 GHz) optical-to-electrical (O-E) bandwidth also serves as the key component. In this project, we have combined the ultra-fast NBUTC-PD (>100 GHz bandwidth) and advanced optical pulse shaper system to demonstrate the (near) real-time MMW (> 100 GHz) arbitrary waveform generation. These results would be of vital importance for next generation high-resolution MMW radar system.

Results:

There are two major topics which we will focus in this project. The first is to further improve the output MMW power, MMW bandwidth, and reliability of photonic emitter itself and the other is to demonstrate sum and difference antenna-patterns with a large operation bandwidth (75-110 GHz; full W-band) by use of advanced optical signal processing technique onto these new developed emitter array. We already have significant achievements in these two topics, which will be discussed in detail as follows:

Regarding with the photonic THz emitters, they are usually composed of ultra-fast uni-traveling carrier photodiodes (UTC-PDs) and metallic waveguides [1,2]. The research group at NTT have demonstrated excellent power/bandwidth performances of these emitters, which are now commercially available[1]. Nevertheless, the bandwidths of waveguide-coupled photomixers are usually limited by the intrinsic bandwidth of the metallic waveguides, and their output power is usually around 5-10 dB lower than that of sub-harmonic frequency multiplier modules, which have a very close bandwidth performance and operate at corresponding MMW bands[2]. In this project, we demonstrate a novel waveguide-coupled photonic THz transmitter capable of overcoming the intrinsic bandwidth limitation of the waveguide which can cover most of the low-loss sub-THz windows for wireless transmission (0.1 to 0.3 THz) [3]. The module is mainly composed of a novel ultrafast uni-traveling carrier PD (UTC-PD) with a type-II hybrid absorber [4], dual ridge horn antenna [5], and planar circuits for waveguide/antenna excitation. By using such a transmitter with the same dual ridge horn antenna in the receiving end, we demonstrate the generation, wireless transmission, and detection of THz wave power with an extremely-wide $\pm$3-dB fractional bandwidth (0.1 to 0.3 THz; 100%). Under a 10 mA output photocurrent, we detect an output power of 31.6 μW at 0.24 THz at the receiving-end.

Figure 1(a) shows the CAD layout for full-wave simulation of the proposed transmitter chip. It is shown that the active PD chip is flip-chip bonded onto a 150-μm thick AlN carrier, where planar passive slotline circuits and a bowtie-shaped waveguide feed are imprinted. The PD-integrated transmitter chip is partially inserted into a WR-6 waveguide with the aid of two alignment grooves on the slotline, and the photo-generated output power from the PD is delivered to the bow-tie radiator for waveguide excitation, as shown in the configuration in Figure 1(b). The entire transmitter module, as depicted in Figure 2, is realized by connecting the WR-6 to a WR-10 based dual ridge horn antenna through a WR-6 to WR-10 waveguide transition. From the microwave network point of view, the entire module is represented as a three-port network, including a photo-generated source input and a 50-Ω matched load as indicated on Fig. 1(b) and the horn opening marked on Fig. 2. The corresponding reflection coefficient, S_{11}, and the transmission coefficient, viz. S_{31}, are extracted at every single frequency of the operating band by means of a co-simulation with the finite-element based full-wave solver, ANSYS HFSS [6], and the high-frequency circuit solver, Keysight ADS [7]. The design approach of the transmitter module is essentially similar to that presented in [8,9], but the upper bound of the operating regime is greatly extended (~300 GHz) thanks to the adopted dual-ridge horn antenna. The planar passive elements used for transmitter chip development, including the notch filter (RF choke), bowtie feed, and tapered slotline between the integrated PD and the feed, are first described below. The design of the dual-ridge horn along with its effect as a load to the transmitted chip is then presented. As shown in Figure 1(a), the RF choke is right below the filp-chip bonded PD chip. With the RF choke, the partially reflected photo-generated source from the bowtie feed is isolated from the PD bias, i.e. a notch filter to block transmission of the photo-generated source.

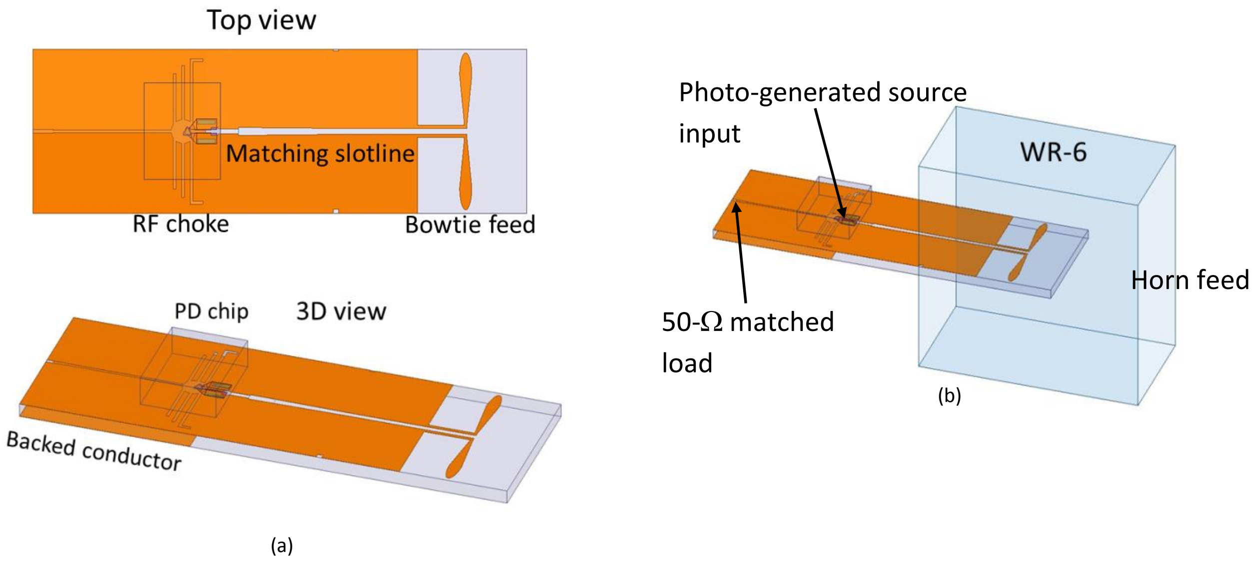

Figure 1. (a) CAD layout of the transmitter chip in our proposed waveguide-coupled photonic transmitter; (b) CAD layout of the feed configuration for the WR-6 waveguide.

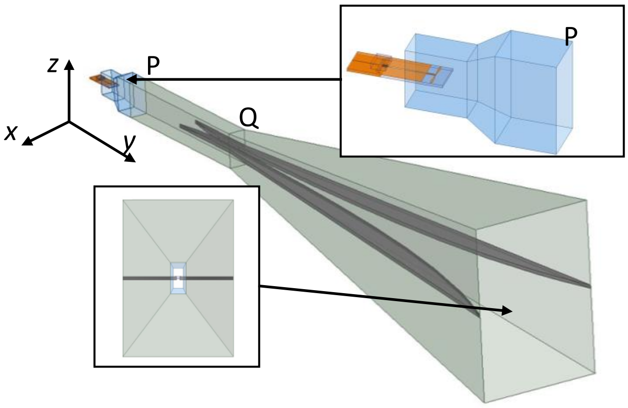

Figure 2. CAD layout of the entire waveguide-coupled photonic transmitter module, including a dual ridge horn antenna.

Figure 3 (a) shows the top view of the fabricated passive circuits together with the bowtie feed on the AlN substrate, as well as the top view of the PD chip. The top view of the entire transmitter chip after flip-chip bonding of the PD onto the substrate is presented in Figure 3 (b). The micro-machined dual-ridge horn antenna is shown on the right of Figure 4, and the point-to-point wireless transmission setup is presented on the left of Figure 4. As shown in Figure 4, a WR-10 based dual-ridge horn is employed as the transmitting/receiving antenna, and the horn is connected to the WR-6 feed via a tapered waveguide. At the receiving end, the received power is measured with a thermal power meter (PM4, VDI-Erickson[2]). The distance between two horn openings is 1 cm.

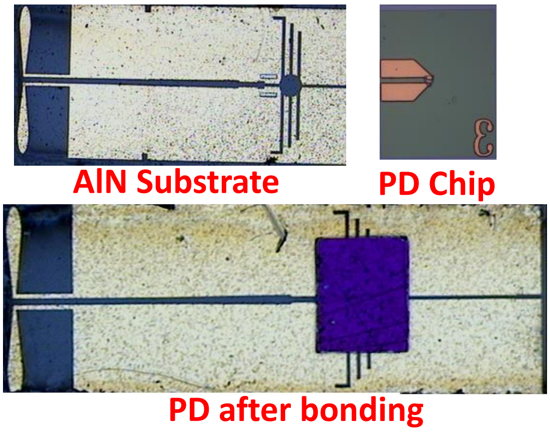

Figure 3. Top-view of the fabricated photonic transmitter chip: (a) before; and (b) after flip-chip bonding.

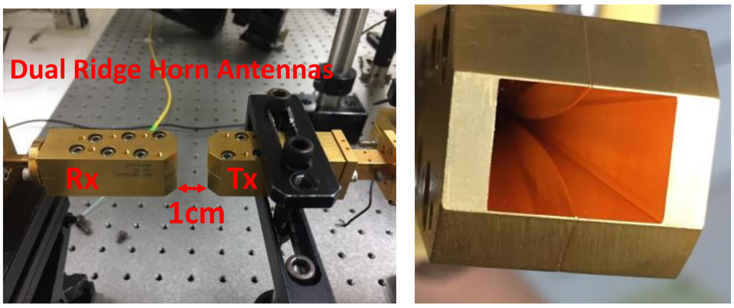

Figure 4. Photo of the wireless transmission setup and the fabricated dual ridge horn antenna.

A typical two-laser heterodyne beating system is adopted in our setup to test the O-E frequency responses and photo-generated THz power from our transmitter. Figures 5 (a) and (b) show the measured O-E frequency response of our PD with active diameters of 3 and 5 μm active, respectively, after flip-chip bonding and under a load of 50 Ohm [6] We can clearly see that for the 3 μm device, under an output photocurrent of 5 mA and an optimum bias of -0.5 V, the measured maximum 3-dB O-E bandwidth can reach 0.33 THz, which meets the bandwidth required for photonic transmitter, as discussed latter. On the other hand, there is a degradation of the 3-dB O-E bandwidth of 5 μm device to 150 GHz due to the decrease in the RC-limited bandwidth [6].

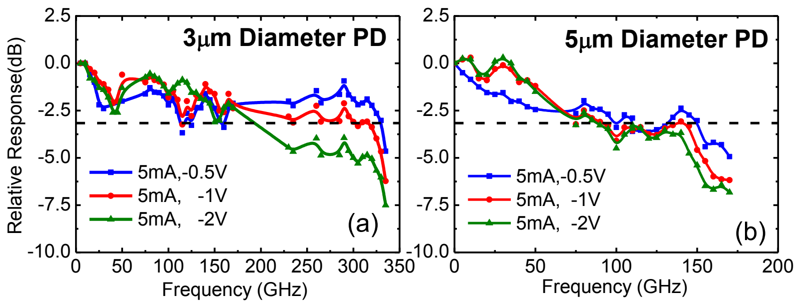

Figure 5. (a) The measured O-E frequency responses of our active PD with: (a) 3; and (b) 5 μm active diameters

Figure 6 (a) shows the measured frequency response of the fully wireless transmitter module at the receiving end. The output photocurrent is fixed at 8 mA during the measurement. Here, the black and green traces represent the measured traces from two different modules (Transmitter 1 and 2) but with the same package and same PD active diameter of 3 μm. We can clearly see that both modules have very similar O-E frequency responses and can cover the 0.1 to 0.3 THz operating frequency. Choosing the detected power at 0.2 THz as a reference point, the measured ± 3-dB optical-to-electrical (O-E) bandwidth can be as wide as 0.2 THz (0.1 to 0.3 THz). This corresponds to a 100% fractional bandwidth. The fractional bandwidth achieved here should be the highest reported among waveguide-coupled photonic transmitters [9,10]. Figure 6 (b) shows the measured frequency response for the same transmitter module but with 3 and 5 μm active diameter PDs packaged inside. As can be seen, under the same output photocurrent (8 mA), the transmitter module with a 3 μm PD exhibits a much better O-E bandwidth than does the 5 μm device due to its much wider O-E bandwidth performance (0.33 vs. 0.15 THz), as discussed above.

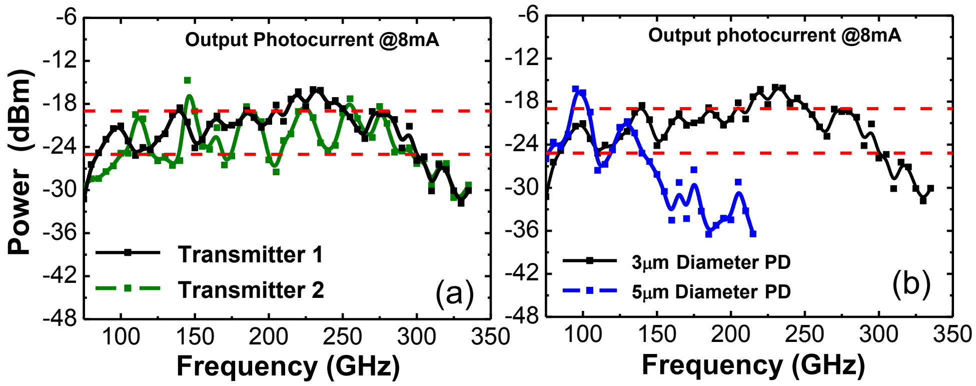

Figure 6. The measured O-E frequency responses of our wireless transmission channel (photonic transmitter with receiving antenna) with: (a) 3 um; and (b) 5 um active diameter PDs packaged into the transmitter module

To demonstrate the performance of the proposed waveguide coupled photomixer, the measured O-E frequency responses, in terms of bandwidth and power, are compared against the ones obtained with a commercially available photomixer. Figure 7 shows the measured O-E frequency responses for our home-made transmitter module (3 um PD inside) and for the commercially available W-band photomixer[1] (IOD-PMW-13001) measured under the same test setup, as shown in Figure 4, and the same output photocurrent of 8 mA. We can clearly see that our home-made device has a broader fractional bandwidth and can attain a higher output power than those of the commercial photomixer when the operating frequency is over 160 GHz. The measurement results reflect the trade-off between output power and fractional bandwidth in the design of waveguide-coupled photomixer.

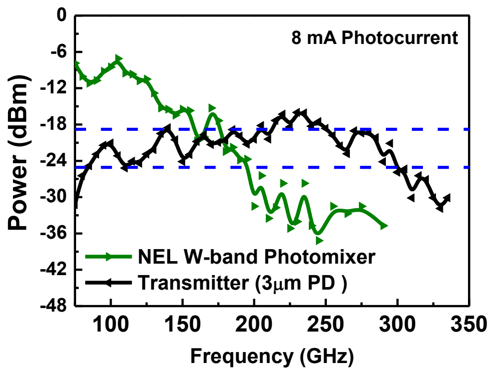

Figure 7. The measured O-E frequency responses for our wireless transmission channel (photonic transmitter with receiving antenna) design obtained using our home-made transmitter (black trace) and the commercial one (green trace).

Figure 8 shows the power measured at the receiving end versus the output photocurrent on the transmitter side. The operating frequency is fixed at 0.24 THz. The red line is the ideal photo-generated THz power versus photocurrent for a 100% optical modulation depth and a 50 Ohm load. The difference between the measured power and the ideal curve represents the summation of 4 dB loss from the non-ideal (~63 %) optical modulation depth in our hetero-dyne beating system [14], radiation loss, and waveguide coupling loss for our setup. We can clearly see that all three tested devices (Tx 1 to Tx 3) showed a close value of maximum detected power at around 31.6 uW with the same saturation current at around 10 mA. A higher receiving power can be expected by installing a Teflon based THz lens to focus the power emitted from transmitting antenna onto the receiving one to minimize the radiation loss [1-3].

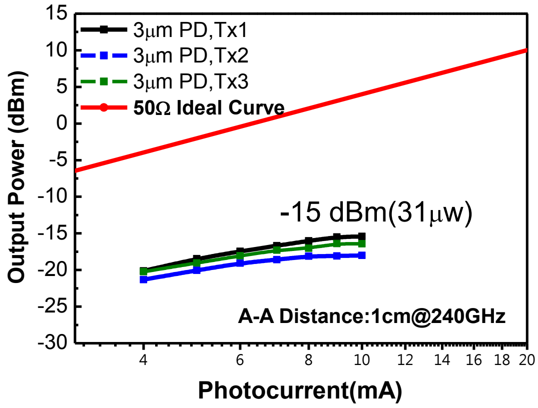

Figure 8. The detected power at the receiving-end at 0.24 THz versus output photocurrent from our photonic transmitters. Tx 1 to Tx 3 represent the three different photonic transmitters with the same packaging, same active PD inside, and under the same test setup.

The other part of this project is to realize ultra-wide bandwidth mono chirped pulse radar based on photonic approach. Compared with radar systems operating in lower frequency bands, a milli-meter wave (MMW)/THz radar system provides higher spatial resolution [12,13], which has important applications for standoff personnel screening [12], autonomous vehicles [14], and intelligent driver assistance systems [15]. Incorporating photonic technologies for generation of MMW/microwave chirped pulses [13,16] offers superior bandwidth performance compared with waveforms demonstrated in traditional chirped pulse radar systems. Large bandwidth can provide high range resolution in a radar system, while the use of waveforms with large time-bandwidth product (TBP) circumvents tradeoffs between transmit energy and range resolution. In order to further attain a high resolution 3-dimensional (3-D) image, the quasi-optics approach, which is based on the MMW/THz lens and parabolic mirror for focusing the MMW beam and narrowing down its spot size, has been successfully demonstrated [12,17]. Nevertheless, the trade-off between resolution and ranging distance becomes an important issue in this approach due to the limited working distance of lens. Monopulse radar is an efficient alternate solution to enhance transverse spatial resolution in traditional radar by using beam forming to obtain a sharp null in the difference far-field pattern of a simple transmitter array (two/four elements for spatial resolution in one/two dimensions) [15,18]. By utilizing wide-band chirped pulse signals in monopulse radar, a high resolution 3-D image can thus be expected. However, the traditional MMW phase shifter, which is an essential component in a monopulse radar system [18] for switching between sum and difference radiation patterns, has difficulty in handling ultrabroadband chirped waveforms with fast and nearly continuous time-varying frequency components. Photonic beamforming with true time delay (TTD) is an alternative solution to eliminate the pulse distortion and frequency (time)-dependent far-field patterns (the squint phenomenon) that arise in transmitter arrays with traditional phase shifters. It has been successfully demonstrated in phased array antenna systems [19,20] in the lower radio frequency (RF) regime with limited bandwidth (up to 1 GHz).

In this project, for the first time, we demonstrate waveform generation suitable for W-band (75-110 GHz) chirped monopulse radar by using a pair of optical pulse shaping based RF arbitrary waveform generators [13] which drive a pair of high-power uni-traveling carrier photodiode (UTC-PD) based photonic transmitters connected to a pair of standard horn antennas for signal emission. Sum and difference patterns with a high extinction ratio (15 dB) across a record 15 GHz bandwidth (80-95 GHz) are achieved. Figure 9(a) shows the setup of the W-band antenna array experiments. It consists of three parts: photonic-assisted arbitrary waveform generation (AWG), fast photo-detection, and wireless antenna array channel. User defined optical profiles, which later through photodetection turn into desired W-band waveforms, are generated by modulating the optical spectrum of a mode-locked laser using pulse shapers based on the near-field frequency-to-time mapping technique [21]. It has been shown that W-band waveforms generated in this way show low phase noise and timing jitter [13]. In the experiment, the optical pulse from the laser source is stretched in time by the dispersive fiber, with 37.5 ps/nm total dispersion. After an input pulse passes through the dispersive fiber, it is divided into two arms by a fiber splitter and spectrally shaped by two pulse shapers; the two optical waveforms in the time domain are the stretched replicas of the tailored power spectra. The two pulse shapers in our setup are programmed independently, each with 500 super-pixels, covering the entire optical C-band (5 THz bandwidth with 10 GHz spectral resolution). The optical signals from the photonic-assisted AWG are converted to millimeter-waves (MMWs) by two UTC-PDs based waveguide-coupled photomixers (one homemade [22], one commercial (NTT Electronics IOD-PMW-13001)). These two waveguide photomixers are connected to two horn antennas which are placed side-by-side, separated by ~2 cm, to serve as the monopulse transmitter. A third horn antenna, which sits on a swing arm controlled by a programmable translation stage, located 3 meters away and facing the two transmitters, serves as the receiver. All three antennas are identical with the same 20 dB antenna gain across the full W-band. To illustrate, the photonic assisted AWG is programmed to generate a linearly chirped W-band waveform, covering 80 to 95 GHz with 1.5 ns time duration and 4 ns repetition period. For simplicity, only one transmitter is enabled. Figure 9(b) shows the down-converted signal at the receiving antenna (with zero angular displacement), recorded by a real-time oscilloscope with a sampling rate of 50 GS/s. The mixer, with ~17 GHz intermediate frequency (IF) bandwidth, down-converts the received chirp signal to 2 – 17 GHz when the local oscillator (LO) frequency is set to 78 GHz. The reconstructed W-band waveform shown in Fig. 9(c) is calculated offline by directly up-converting the spectrum of the waveform shown in Fig. 9(b) by the LO frequency and inverse Fourier transforming.

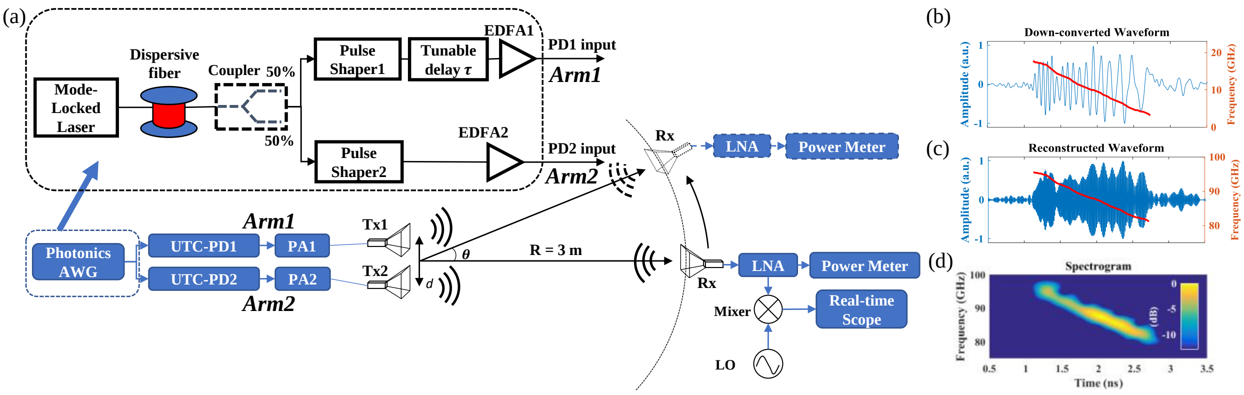

Fig. 9. Experimental arrangement and wireless W-band waveform transmission with ultrabroad bandwidth. (a) Setup schematic. EDFA, erbium doped fiber amplifier; PD, photodiode; AWG, arbitrary waveform generation; UTC-PD, uni-traveling carrier photodiode based waveguide-coupled photomixer; PA, power amplifier; Tx, transmitter; Rx, receiver; LNA, low noise amplifier, LO, local oscillator; d = 2 cm, R = 3 m. (b) W-band chirp signal from a single transmitterand its instantaneous center frequency, measured at the receiver end after down-conversion, showing 15 GHz bandwidth. Transmitted chirp, 80 – 95 GHz. LO frequency, 78 GHz. (c) Reconstructed received W-band chirp signal and its instantaneous center frequency. (d) Spectrogram of (c).

We now demonstrate operation of the 2-element antenna transmitter array. In phase and out of phase interference is first investigated in the time domain. The two pulse shapers are programmed to generate the W-band waveforms described in the last paragraph, but with either the same or opposite polarities. The transmitted waveforms are measured one at a time at the receiving antenna, which is set to the center of the transmitter axis with angular offset $\theta = 0°$, as shown in Fig. 9(a). The down-converted RF waveforms are shown in Fig. 10(a) for opposite polarity and in Fig. 10(b) for the same polarity. The ability to impose a uniform π phase shift (polarity change) across the entire 15 GHz bandwidth is clearly visible. Figure 10(c) shows the down-converted received waveforms with both transmitters operating simultaneously. For the same polarity case (red), constructive interference of the two transmit signals across the entire waveform is observed; for the opposite polarity case (blue), destructive interference occurs. The destructive interference trace shows minimum amplitude over the entire time aperture, while the amplitude of the constructive interference trace doubles that of the single-transmitter case. In addition, the RF power spectra over the down-converted frequency band are obtained via offline computation and displayed in Fig. 10(d). The average extinction ratio over 2-17 GHz (corresponding to 80-95 GHz in the W-band) between the in-phase (solid red) and the out-of-phase (solid blue) is 15.96 dB. Moreover, the amplitude doubling shown in Fig. 10(c) in red appears in Fig. 10(d) in the form of ~6 dB gain between the in-phase interference (solid red) and the single-Tx (dashed lines) power spectra.

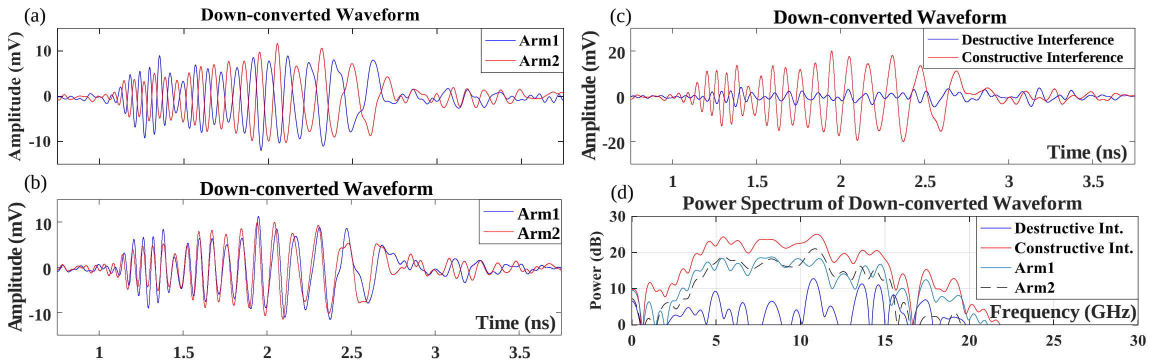

Fig. 10. Far-field antenna array measurement in the time domain. (a): Down-converted waveform at Rx when Tx1 on Tx2 off (blue), Tx1 off Tx2 on (red). Feeding waveforms for Tx1 and Tx2 are out of phase. (b): Similar to (a) but feeding waveform for Tx1 and Tx2 are in phase. (c): Down-converted sum (red) and difference (blue) interference waveforms at Rx when both Tx are switched on. (d) Spectrum analysis of received signal. Red

solid, Tx1 and Tx2 are in phase and both switched on. Blue solid, Tx1 and Tx2 are out of phase and both switched on. Green dash, Tx1 on and Tx2 off. Black dash, Tx1 off and Tx2 on.

To illustrate spatial manipulation of the far-field antenna pattern, the previously described chirps are measured at the receiver using a W-band power meter, which gives the W-band power integrated over frequency (time). The far-field pattern is acquired by stepwise sweeping the receiver antenna over an arc, from $\theta = -30°$ to $+30°$ with a $0.25°$ angular increment. The measurement is conducted in both the sum and difference scenarios. The obtained results are plotted in Figs. 11 (e) – (c). In the difference interference case, both the polar (Fig. 11(a)) and Cartesian (Fig.11(b)) plots show a null at the center. On the contrary, when the transmitters broadcast chirps with the same polarity, a constructive peak is observed at $\theta = 0$, shown in Fig. 11(c) and (d). An extinction ratio of 15.31 dB between the sum and difference patterns at $\theta = 0$ is observed, in excellent agreement with the extinction ratio estimated from the time domain data (Fig. 10).

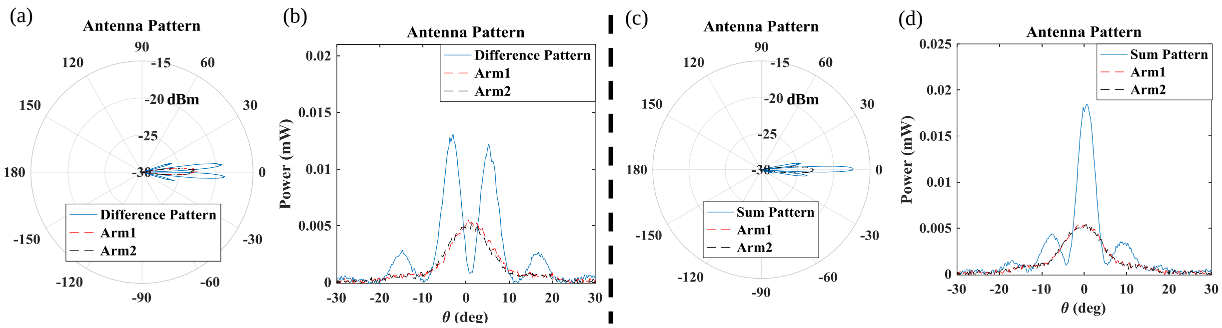

Fig. 11. Far-field antenna pattern measurement. (a,b) Far-field (3 m) broadband antenna array pattern with Tx1 and Tx2 out of phase. Polar plot with log scale in (a) and Cartesian plot with linear scale in (b). (c,d) Far-field (3 m) broadband antenna array pattern with Tx1 and Tx2 in phase. Polar plot with log scale in (c) and Cartesian plot with linear scale in (d). The measured powers at $\theta = 0$ are 0.65 μW and 22.1 μW for out-of-phase and in-phase transmission, respectively; the power at $\theta = 0$ with only a single transmitter enabled is 5.81 μW.

In summary, we use photonic-assisted arbitrary waveform generation and waveguide-coupled UTC photomixers to drive a two-element antenna array with 15 GHz chirp waveforms in the W-band frequency region. By changing the relative polarity of the drive waveforms, we have achieved constructive and destructive interference of the on-axis radiation with 15 dB average contrast over 80-95 GHz. Far-field antenna array patterns are also acquired, proving the capability of focusing energy in different spatial directions by changing the phase between two broadband transmit waveforms. In continuing work we are interested to explore angular scanning of the broadband in-phase and out-of-phase radiation patterns via true time delay adjustment of the drive signals and to pursue actual monopulse radar operation by transmitting the broadband in-phase and out-of-phase radiation at a target and analyzing the scattered return signals at the third antenna with the down-converting receiver.

References

[1] A. Wakatsuki, T. Furuta, Y. Muramoto, T. Yoshimatsu, and H. Ito, "High-power and Broadband Sub-terahertz Wave Generation Using a J-band Photomixer Module with Rectangular-waveguide Output Port," *Tech. Dig. 2008 Infrared, Millimeter and Terahertz Waves (IRMMW-THz 2008)*, pp. M4K2 1199, Sep., 2008.

[2]T. Ishibashi, Y. Muramoto, T. Yoshimatsu, and H. Ito, "Unitraveling-Carrier Photodiodes for Terahertz Applications," *IEEE J. of Sel. Topics in Quantum Electronics*, vol. 20, pp. 3804210, Nov./Dec., 2014.

[3] C. C. Renaud, M. Natrella, C. Graham, J. Seddon, F. V. Dijk, and A. J. Seeds "Antenna Integrated THz Uni-Traveling Carrier Photodiodes," *IEEE J. of Sel. Topics in Quantum Electronics*, vol. 24, No. 2, pp. 8500111, March,/April, 2018.

[4] H. Ito and T. Ishibashi, "Photonic Terahertz-Wave Generation Using Slot-Antenna-Integrated Uni-Traveling-Carrier Photodiodes," *IEEE J. of Sel. Topics in Quantum Electronics*, vol. 23, pp. 3800907, July/August, 2017.

[5] J. Wells, "Faster Than Fiber: The Future of Multi-Gb/s Wireless," *IEEE Microwave Magazine*. vol. 10, pp. 104-112, May, 2009.

[6] J.-M. Wun, Y.-W. Wang, and J.-W. Shi, "Ultra-Fast Uni-Traveling Carrier Photodiodes with $GaAs_{0.5}Sb_{0.5}/In_{0.53}Ga_{0.47}As$ Type-II Hybrid Absorbers for High-Power Operation at THz Frequencies," *IEEE J. of Sel. Topics in Quantum Electronics*, vol. 24, No. 2, pp. 8500207, March,/April, 2018.

[7] V. Rodriguez, "The dual-ridged horn antenna," *EE, Evaluation engineering* vol. 45, No. 10, pp. 58-63, Oct., 2006.

[8] ANSYS HFSS:3D full-wave electromagnetic field simulation, ANSYS, Inc.

[9] Keysight ADS, Keysight Technologies, 1400 Fountaingrove Parkway, Santa Rosa, CA 95403-1799.

[10] N.-W. Chen, H.-J. Tsai, F.-M. Kuo, and J.-W. Shi, "High-Speed W-Band Integrated Photonic Transmitter for Radio-Over-Fiber Applications," *IEEE Trans. Microwave Theory Tech.*, vol. 59, No. 4, pp. 978-986, April, 2011.

[11] N.-W. Chen, J.-W. Shi, F.-M. Kuo, J. Hesler, T. W. Crowe, and J. E. Bowers, "25 Gbits/sec Error-Free Wireless Link between Ultra-Fast W-Band Photonic Transmitter-Mixer and Envelop Detector," *Optics Express*, vol. 20, No. 19, pp. 21223-21234, Sep., 2012.

[12] K. B. Kooper, R. J. Dengler, N. Llombart, T. Bryllert, G. Chattopadhyay, E. Schlecht, J. Gill, C. Lee, A. Skalare, I. Mehdi, and P. H. Siegel, “Penetrating 3-D Imaging at 4- and 25-m Range Using a Submillimeter-Wave Radar” *IEEE Trans. on Microwave Theory Tech.*, vol. 56, pp. 2771-2778, Dec, 2008.
[13] Y. Li, A. Rashidinejad, J.-M. Wun, D. E. Leaird, J.-W. Shi, and A. M. Weiner, “Photonic Generation of W-band Arbitrary Waveforms with High Time-Bandwidth Products Enabling 3.9mm Range Resolution,” *Optica*, vol. 1, no. 6, pp. 446-454, Dec., 2014
[14] M. Kishida, K. Ohguchi, M. Shono, “79 GHz-Band High-Resolution Millimeter-Wave Radar,” *Fujitsu Sci. Tech. J.*, vol. 51, no. 4, pp. 55-59, Oct., 2015.
[15] P. Molchanov, S. Gupta, K. Kim, and K. Pulli, “Short-Range FMCW Monopulse Radar for Hand-Gesture Sensing” *IEEE Radar Conference* Arlington, VA, USA, May, 2015, pp. 1491-1496.
[16] C. Wang and J. Yao, “Photonic Generation of Chirped Millimeter-Wave Pulses Based on Nonlinear Frequency-to-Time Mapping in a Nonlinearly Chirped Fiber Bragg Grating,” *IEEE Trans. on Microwave Theory Tech.*, vol. 56, pp. 542-553, Feb., 2008.
[17] Tzu-Fang Tseng, Jhih-Min Wun, Wei Chen, Sui-Wei Peng, Jin-Wei Shi, and Chi-Kuang Sun,“High-depth-resolution 3-dimensional radar-imaging system based on a few-cycle W-band photonic millimeter-wave pulse generator,” *Optics Express*, vol. 21, No. 12, pp. 14109-14119, June, 2013.
[18]S. Wang, K.-H. Tsai, K.-K. Huang, S.-X. Li, H.-S. Wu, and C.-K. C. Tzuang, “Design of W-band RF CMOS Transceiver for FMCW Monopulse Radar,” *IEEE Trans. on Microwave Theory Tech.*, vol. 57, no. 1, pp. 61-70, Jan., 2009.
[19] J. Yao, “Microwave Photonics,” *IEEE/OSA Journal of Lightwave Technology*, vol. 27, pp. 314-335, Feb., 2009.
[20] R. Rotman, M. Tur, and L. Yaron, “True Time Delay in Phased Arrays,” *Proc. of the IEEE* vol. 104, no. 3, pp. 504-518, March, 2016.
[21] A. Dezfooliyan and A. M. Weiner, "Photonic synthesis of high fidelity microwave arbitrary waveforms using near field frequency to time mapping", Opt. Exp., vol. 21, no. 19, pp. 22974-22987, 2013.
[22] Nan-Wei Chen, Jin-Wei Shi, Fong-Ming Kuo, Jeffery Hesler, Thomas W. Crowe, and John E. Bowers, “25 Gbits/sec Error-Free Wireless Link between Ultra-Fast W-Band Photonic Transmitter-Mixer and Envelop Detector,” *Optics Express*, vol. 20, No. 19, pp. 21223-21234, Sep., 2012.

Publications

Journal

1. Yi-Han Chen, Jhih-Min Wun, Song-Lin Wu, Rui-Lin Chao, Jack Jia-Sheng Huang, Yu-Heng Jan, H.-S. Chen, C.-J. Ni, Hsiang-Szu Chang, Emin Chou, and Jin-Wei Shi, “Top-Illuminated $In_{0.52}Al_{0.48}As$-Based Avalanche Photodiode with Dual Charge Layers for High-Speed and Low Dark Current Performances,” *IEEE J. of Sel. Topics in Quantum Electronics*, vol. 24, No. 2, pp. 3800208, March/April., 2018.

2. J.-M. Wun, Y.-W. Wang, and J.-W. Shi, “Ultra-Fast Uni-Traveling Carrier Photodiodes with $GaAs_{0.5}Sb_{0.5}/In_{0.53}Ga_{0.47}As$ Type-II Hybrid Absorbers for High-Power Operation at THz Frequencies,” *IEEE J. of Sel. Topics in Quantum Electronics*, vol. 24, No. 2, pp. 8500207, March,/April, 2018.

3. Nan-Wei Chen, Jhih-Min Wun, Hao-Chen Wang, Rui-Lin Chao, Chris Koh, C. H. Dreyfus and Jin-Wei Shi, “Design and Analysis of Waveguide-Coupled Photonic THz Transmitters with an Extremely Wide Fractional Bandwidth,” to be published in *IEEE/OSA Journal of Lightwave Technology*, vol. 36, Oct., 2018. (Special Issue on Microwave Photonics) 10.1109/JLT.2018.2808932

Conference

1. Bohao Liu, Jhih-Min Wun, Nathan P O'Malley, D. E. Leaird, Nan-Wei Chen, Jin-Wei Shi, and Andrew M. Weiner, “Extremely Wide Bandwidth Microwave Photonic Phase Shifter for W-band Chirped Monopulse Radar,” *Proc. OFC 2018, San Diego*, CA, USA, March, 2018, pp. Th3G.6.